Supporting Information

Structural effects of m^{6}A modification of the Xist A-repeat AUCG tetraloop and its recognition by YTHDC1

Alisha N. Jones[1,2,†], Ekaterina Tikhaia[1,2,†], André Mourão[1,2] and Michael Sattler[1,2*]

[1] Institute of Structural Biology, Helmholtz Zentrum München Ingolstädter Landstr. 1, 85764 Neuherberg, Germany.

[2] Bavarian NMR Center, Department of Chemistry, Technical University of Munich, Lichtenbergstr. 4, 85747, Garching, Germany.

[*] To whom correspondence should be addressed. Tel: +49 (0)89 289 52600;
Email: sattler@helmholtz-muenchen.de

† Joint Authors

Content:

Supplementary Figure 1

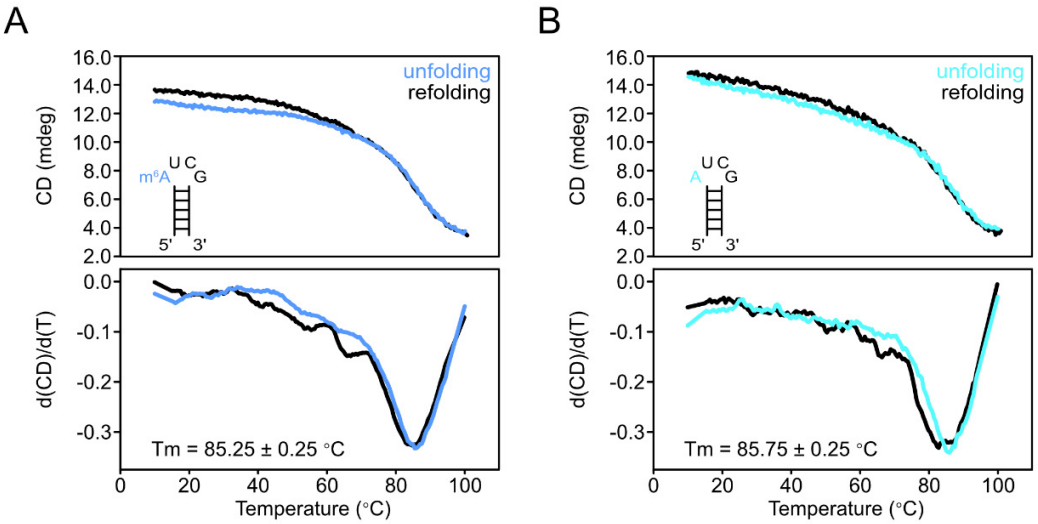

Supplementary Figure 1. **(A)** CD-monitored unfolding (blue) and refolding (black) profiles for the (m^6A)UCG tetraloop hairpin (top) recorded in NMR buffer (25 mM sodium phosphate buffer pH 6.4, 25 mM NaCl) and their first derivative curves (bottom). **(B)** CD-monitored unfolding (cyan) and refolding (black) profiles for the AUCG tetraloop hairpin (top) recorded in NMR buffer and their first derivative curves (bottom).

Supplementary Figure 2

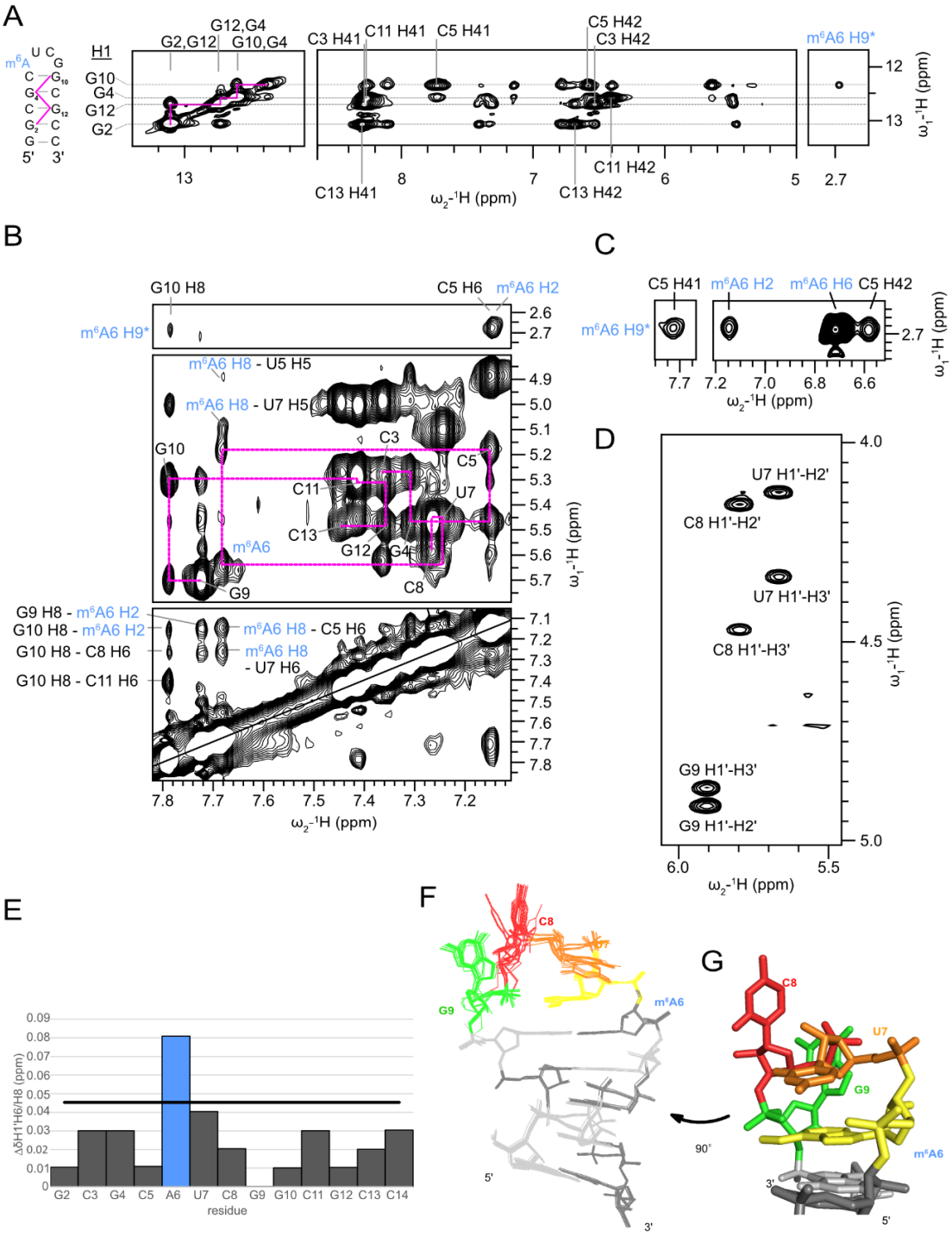

Supplementary Figure 2. (A) Homonuclear ^{1}H-^{1}H NOESY spectra (280K) of imino proton resonances and corresponding NOEs to amino and m^{6}A methyl protons. **(B)** ^{1}H-^{1}H NOESY spectra showing NOEs from the m^{6}A methyl protons to aromatic protons, and the H1'-H6/H8 sequential NOE walk. **(C)** NOEs between the methyl group of m^{6}A with exchangeable amino protons of both C5 and m^{6}A seen in ^{1}H-^{1}H NOESY spectra collected in H_2O. **(D)** Homonuclear ^{1}H-^{1}H TOCSY spectrum (280K) of ribose H1'

correlations with H2' and H3' protons. U7, C8, and G9 show strong correlations, indicative of C2'-endo ribose conformation. **(E)** Chemical shift perturbation (CSP) highlighting resonances that undergo significant chemical shift changes upon N^6 methylation of A6 for H1', H6 and H8 chemical shifts. The solid horizontal line represents the average chemical shift perturbation plus one standard deviation. **(F)** Ensemble of the 10 lowest energy structural models of the (m^6A)UCG tetraloop hairpin. **G)** Side view of the lowest energy structure of (m^6A)UCG tetraloop.

Supplementary Figure 3

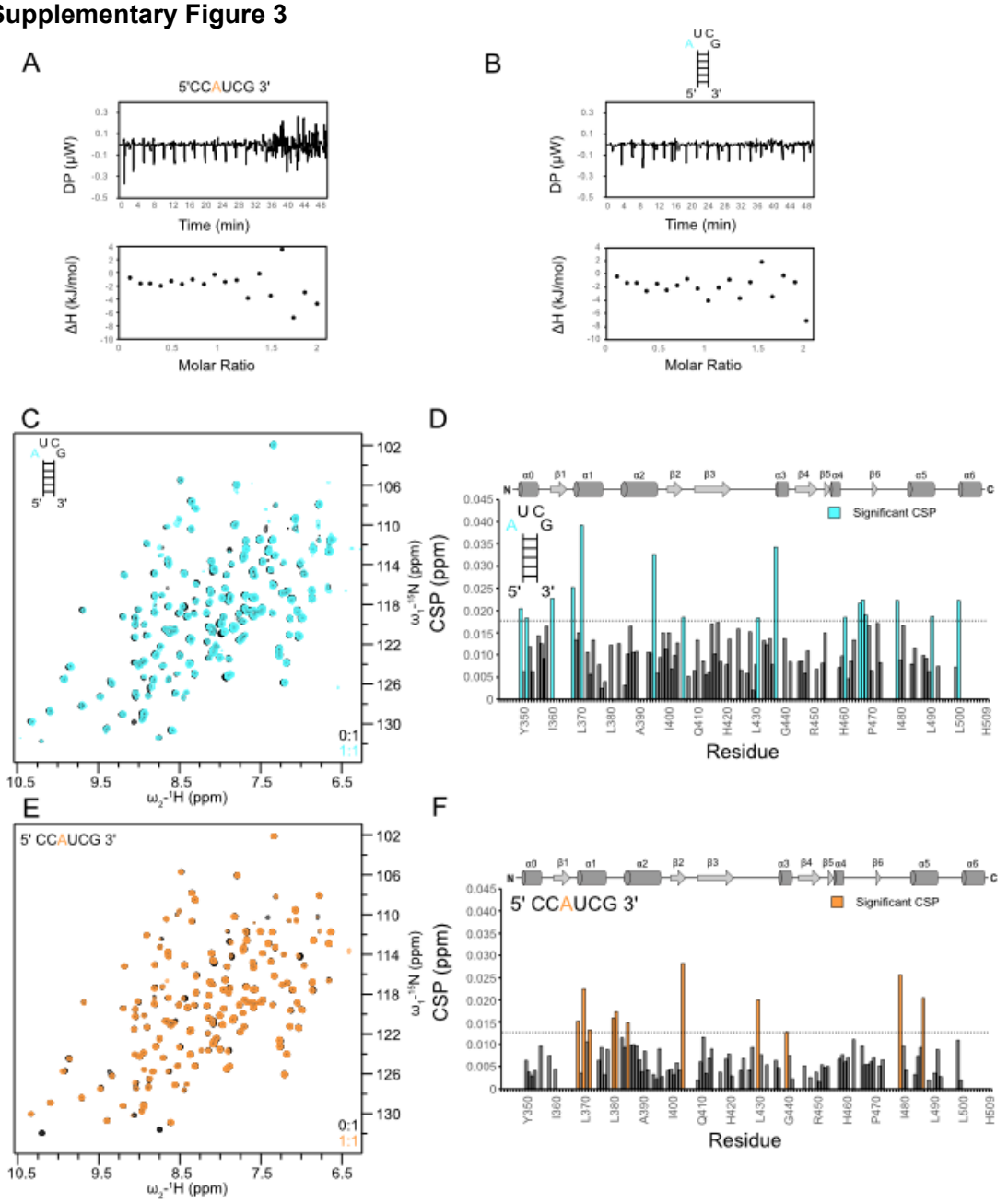

Supplementary Figure 3. ITC heat plot and binding curve for the interaction of the YTH domain with the **(A)** single-stranded Xist CCAUCG hexamer RNA and **(B)** and the Xist AUCG tetraloop hairpin. **(C)** ^{1}H-^{15}N correlation spectra of ^{15}N-labeled YTH domain alone (black) and in the presence of equimolar unlabeled AUCG tetraloop hairpin RNA (cyan). **(D)** Chemical shift perturbation plot highlighting residues that are most strongly affected (cyan) in the presence of the RNA. **(E)** ^{1}H-^{15}N correlation spectra of ^{15}N-labeled YTH domain protein alone (black) and in the presence of equimolar unlabeled Xist CCAUCG hexamer RNA (orange). **(F)** Chemical shift perturbation plot showing residues that are most strongly shifting (orange) in the presence of RNA ligand. The dotted horizontal lines in (D) and (F) represent the average chemical shift perturbation plus one standard deviation.

Supplementary Figure 4

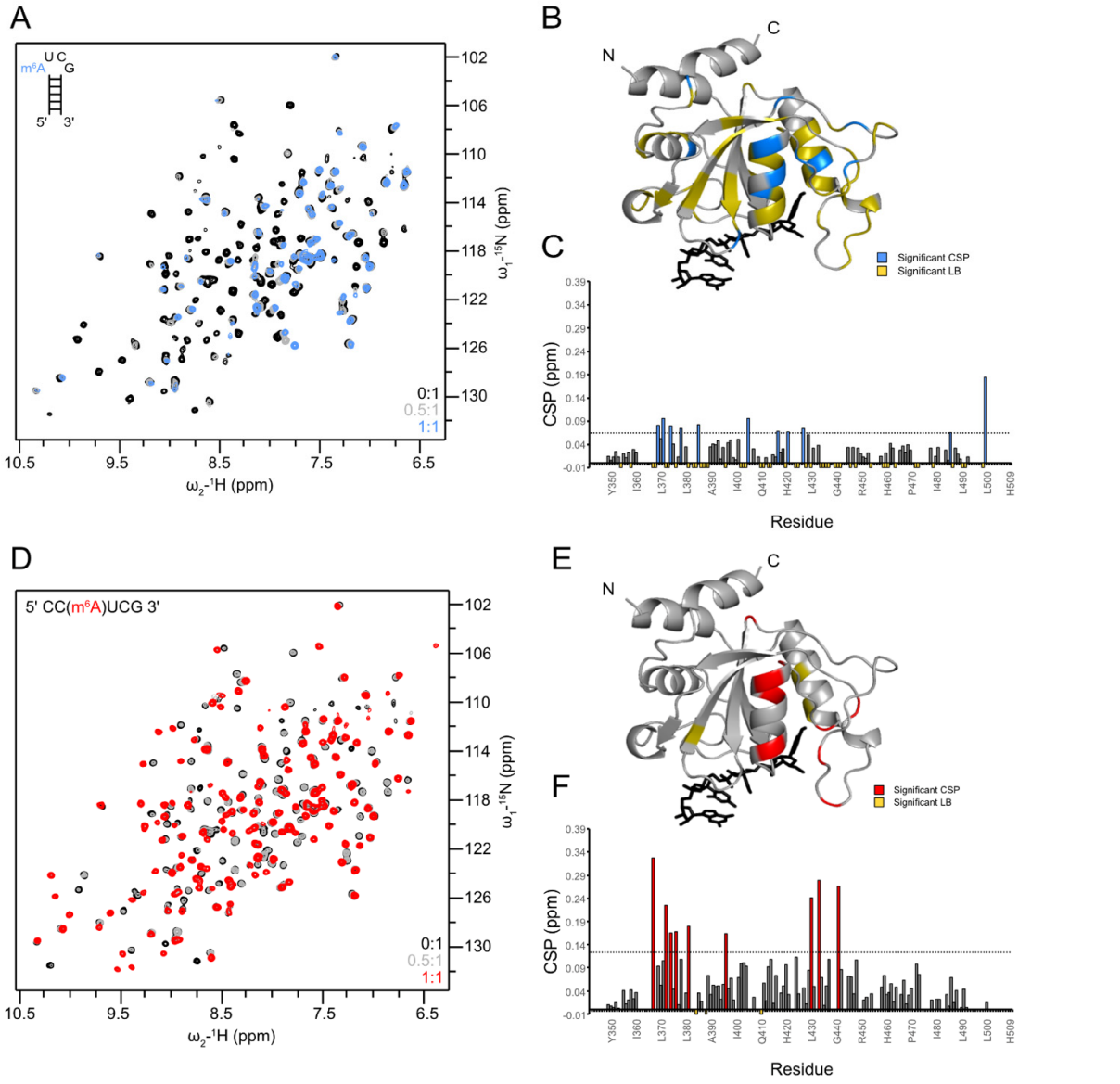

Supplementary Figure 4. **(A)** ^{1}H-^{15}N correlation NMR spectra of ^{15}N-labeled YTH domain free (black) and in the presence of unlabeled (m^{6}A)UCG tetraloop hairpin RNA at 0.5:1 (grey) and 1:1 (blue) RNA-protein ratio. **(B)** Significant CSPs (blue) and line broadening (yellow) mapped to the YTH domain in complex with (m^{6}A)UCG tetraloop hairpin RNA (shown in black). **(C)** Chemical shift perturbation (positive bars) and intensity (negative bars) plot showing residues that are most strongly shifting (blue) or experiencing line broadening, LB, (yellow) in the presence of RNA ligand. **(D)** ^{1}H-^{15}N correlation NMR spectra of ^{15}N-labeled YTH domain free (black) and in the presence of unlabeled single-stranded CC(m^{6}A)UCG hexamer RNA at 0.5:1 (grey) and 1:1 (red) RNA-protein ratio. **(E)** Significant CSPs (red) and line broadening (yellow) mapped to the YTH domain in complex with (m^{6}A)UCG tetraloop hairpin RNA (shown in black). **(F)** Chemical shift perturbation (positive bars) and intensity (negative bars) plot showing residues that are most strongly shifting (red) or broadening (yellow) in the presence of RNA ligand. The dotted horizontal lines in (C) and (F) represent the average chemical shift perturbation plus one standard deviation.

Supplementary Figure 5

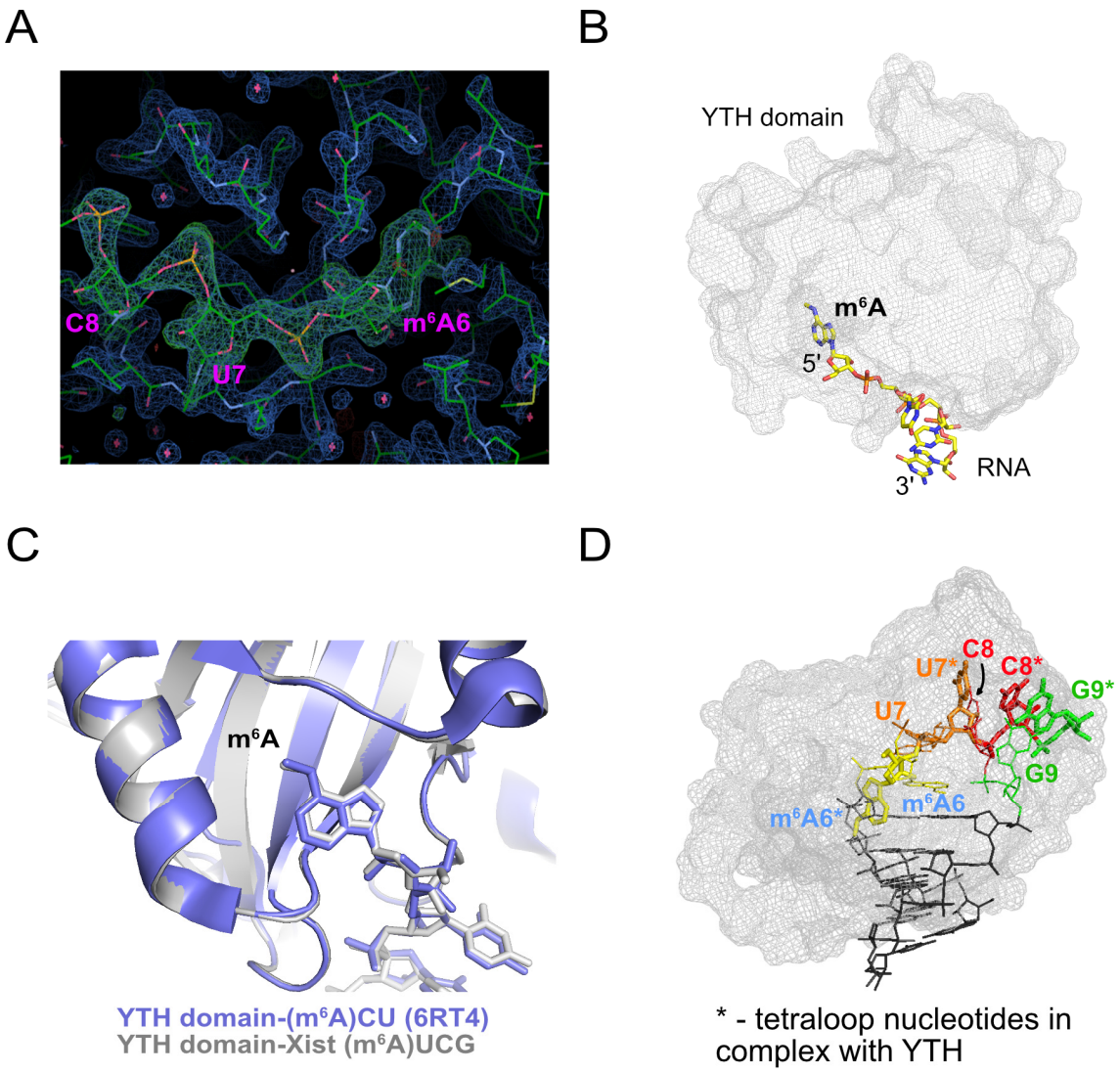

Supplementary Figure 5. **(A)** Electron density for the RNA in the YTH-RNA complex. The unbiased F_o-F_c electron density map shown in green at 3.6 σ visualizes the RNA (annotated in magenta). **(B)** Overview of crystal structure of the YTH domain bound to the region of the (m^{6}A)UCG tetraloop residues with observable electron density. **(C)** Structural superposition of heavy atoms in the YTH domain bound to single-stranded m^{6}ACU RNA (PDB ID 6RT4, lilac) and the crystal structure of the YTH domain bound to the Xist (m^{6}A)UCG tetraloop nucleotides (grey). **(D)** Conformation of the loop nucleotides in the Xist (m^{6}A)UCG hairpin seen in the crystal structure when bound to YTHDC1 (labels marked with an asterisk), superimposed with the unbound m^{6}A hairpin structure. The structures are aligned based on the backbone atoms in the loop in the RNA. The stem residues from the unbound RNA hairpin are indicated as black lines. Note, that this orientation is not compatible with a recognition of the loop by YTH, as the remaining stem region in the m^{6}A hairpin would sterically clash with the YTH domain.

Supplementary Figure 6

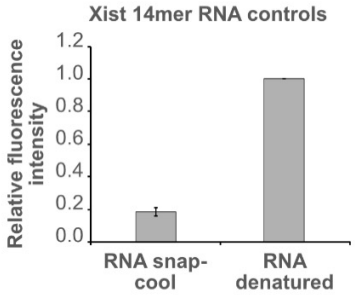

Supplementary Figure 6. Control fluorescence experiments with Xist AUCG tetraloop hairpin; left shows the RNA in the folded state (low emission intensity) and the unfolded/denatured state (high emission intensity) on the right.